



Analysis of Causes of Vibration Differences Induced by Different Kinds of Blastholes Based on the Interpretation of Blasting Parameters: A Case Study in Dam Foundation Excavation

Haixiao Zhou¹ · Qidong Gao^{1,2} · Yong Fan² · Wenbo Lu³ · Yaqiong Wang¹ · Yubo Yang¹ · Zhendong Leng⁴

Received: 30 November 2022 / Accepted: 3 July 2023 / Published online: 13 July 2023

© The Author(s), under exclusive licence to Springer-Verlag GmbH Austria, part of Springer Nature 2023

Abstract

The vibration characteristics induced by different kinds of blastholes, such as presplitting blastholes, smooth blastholes, and production blastholes, are quite different. Figuring out the vibration differences of different kinds of blastholes and the inherent causes are of great significance for the safety control of blast vibration. In this study, taking the excavation of a dam foundation as a case study, the inherent causes of vibration differences induced by presplitting blastholes, smooth blastholes, and production blastholes are investigated and discussed with both theoretical analyses and numerical simulation methods. In addition, onsite blasting experiments are conducted to verify the vibration characteristics differences. The results show that the explosion pressure applied on the hole wall of the presplitting and smooth blastholes are much smaller than those applied on the production blastholes. Thus, the inner blasting effects (i.e., the rock breakage and plastic zone around the blasthole) of the presplitting and smooth blastholes are relatively weaker. On the other hand, the outer blasting effects (i.e., the rock breakage induced by the reflection of blast waves at the free surface) of the presplitting blasthole are negligible because of their substantially larger burden thicknesses relative to the other blastholes. Therefore, much more explosion energy of the presplitting blasthole is converted into vibration energy than the other two kinds of blastholes. However, the vibration energy conversion and the plastic zone development of the smooth blastholes and production blastholes are approximately at the same level due to the balance of their inner and outer blasting effects. The measured peak particle velocities (PPVs) and dominant frequencies induced by different kinds of blastholes show good agreement with the above theoretical and numerical conclusions. It can be drawn that the inherent causes of the vibration characteristics differences induced by various blastholes lie in the differences in the blasting parameters, which determine the proportions of the inner and outer blasting effects.

Highlights

- The inner and out blasting parameters of different kinds of blastholes in dam foundation blasting excavation were defined based on the mechanisms of rock breakage by blasting.
- The blasting vibration responses of rock mass under different blasting parameters were investigated to figure out the inherent causes of vibration characteristics differences of various blastholes.
- Horizontal smooth blasting experiment and horizontal presplitting blasting were carried out to verify the vibration characteristics differences induced by various blastholes.
- We suggest adjusting the inner and outer blasting parameters of blastholes based on the distances of the structures from the explosive sources to minimize the disturbance caused by blasting to structures.

✉ Qidong Gao
qdgao@chd.edu.cn

¹ School of Highway, Chang'an University, Xi'an 710064, Shaanxi, China

² Hubei Key Laboratory of Construction and Management in Hydropower Engineering, China Three Gorges University, Yichang 443002, Hubei, China

³ State Key Laboratory of Water Resources and Hydropower Engineering Science, Wuhan University, Wuhan 430072, China

⁴ Gezhouba Group Explosive Co, Ltd, Chongqing 401121, China

Keywords Rock blasting · Vibration differences · Different kinds of blastholes · Blasting parameters · Dam foundation excavation

1 Introduction

Rock breakage and fragmentation by drilling and blasting have been widely used for foundation excavation in projects of hydropower station, nuclear power plant, municipal engineering, and subgrade production (Ainalis et al. 2016; Yang et al. 2016; Katsabanis 2020). To minimize the adverse effects of blasting vibration and to form a flat blasting profile, the contour blasting (i.e., presplitting blasting and smooth blasting) has been extensively adopted in practical engineering (Yang et al. 2021; Lu et al. 2012). However, the types of blastholes used in various contour blasting techniques are different resulting in different blasting vibration characteristics, which may have deleterious effects on the stability of rock foundations and adjacent structures. Therefore, to control the adverse effects of blasting vibration, it is necessary to make distinction between the various blastholes and figure out the inherent causes for their vibration characteristics differences.

Rock mass dynamic response presents significant differences in the presence of different kinds of blastholes in contour blasting, which have gained more attention by researchers and engineers in recent years. Yang et al. (2016) studied the vibration characteristics differences induced by cutting blastholes and production blastholes in full-face tunnel blasting excavation through onsite experiment and numerical simulation. Their studies indicated that the production blastholes are initiated under another firing condition which the cutting blastholes does not have, i.e. the free surfaces created by the blast of the former delay. Therefore, when the production blastholes are blasted, the reflection waves become considerably stronger due to the increased number of free surfaces, which reduce the duration and peak values of loading pressure in the vicinity of the blasting source, further influencing the blast vibration characteristics. Zhou et al. (2019) conducted a series of experiments of smooth blasting and presplitting blasting in rock well excavation to investigate the vibration characteristics induced by different kinds of blastholes. In their field tests, the researchers claimed that the dominant frequencies induced by smooth blastholes consistently decrease as the distance from the explosion source increases, whereas the dominant frequencies induced by presplitting blastholes might decrease first, followed by a rise. Furthermore, Hu et al. (2014) investigated the damage processes in high rock slope excavation by smooth blasting and presplitting blasting using numerical modeling with cumulative damage materials. They stated that the production blastholes, smooth blastholes, and

buffering blastholes have significant influences on the final damage of the surrounding rock mass in smooth blasting.

For presplitting blasting, the presplitting blastholes are initiated at the first row to generate presplitting cracks, which can effectively reduce the damage induced by the production blastholes. However, the presplitting blastholes are adjacent to reserved rock mass, and their burden thickness is much greater than that of production blastholes, which increases the acting time of the blasting load. So, the final damage of the surrounding rock mass is mainly caused by the presplitting blastholes. Yang et al. (2012) studied the vibration characteristics induced by production blastholes and presplitting blastholes by regression analysis. In their studies, they concluded that, over a distance range of 20 m to 200 m from the explosion sources, the dominant frequencies induced by presplitting blastholes are substantially larger than those induced by producing blastholes.

When the explosives in blastholes are fired, the firing conditions that are sensitive to the blasting effects, such as the burden thickness, initiation mode, free surface, and charge structure, can be defined as blasting parameters. Under different blasting parameters, the vibration characteristics are significantly different. Sanchidrián et al. (2007) conducted a series of experiments to compare the distribution of explosion energy under different burden thicknesses. In their field tests, they claimed that approximately 9% of the explosion energy is converted into vibration energy when the blastholes are initiated under a large burden thickness, a value much higher than that of production blastholes. In addition, under different burden thicknesses, the vibration amplitude spectrums are also different, further influencing the distribution of dominant frequencies. Shi and Chen (2009) compared the dominant frequencies of blasting vibration under various burden thicknesses based on field monitoring data from copper mine blast excavation and found that the dominant frequencies gradually decrease as the burden thickness increases. Singh (1993) studied the relationship between peak particle velocities (PPVs) and distance from the blast center for various decoupling ratios. The researchers stated that the PPV prediction equation can be optimized by incorporating the decay factor about the decoupling ratio. Sun et al. (2021) compared the dominant frequencies under different charge structures and noted that a smaller decoupling ratio leads to a larger initial value of the dominant frequency. Sastry and Ram Chandar (2004) studied the vibration characteristics under different initiation modes. The experimental results demonstrate that the blast-induced PPVs under lateral initiation by detonating cord are much greater than those of end initiation by detonator for the

same scale distance. Gao et al. (2019a) investigated the distribution and utilization of explosion energy under different initiation positions in cylindrical blastholes and found that the PPVs under end initiation are smaller than those under top initiation.

In previous studies, most researchers believed that the pre-splitting cracks and the quality of the explosives in one shot determine the vibration characteristics differences of various blastholes (Li et al. 2016; Yang et al. 2021; Abiodun et al. 2021). However, the quality of the explosives of presplitting blastholes and smooth blastholes are at the same level, and both of them are detonated without pre-splitting cracks. But their vibration characteristics are also different (Yang et al. 2021). Except for the pre-splitting cracks and the quantity of explosives in one shot, the blasting parameters of different kinds of blastholes are also different, which may cause differences in vibration characteristics. Nevertheless, few literatures can be found to investigate the inherent causes of the vibration characteristics differences induced by different kinds of blastholes from the perspectives of blasting parameters.

The first stage of the present study was the analysis of the definitions and differences of blasting parameters for various blastholes. Subsequently, the influences of blasting parameters on explosion energy distribution and plastic zone development were investigated to derive the differences in vibration characteristics induced by various types of blastholes. In addition, the FEM software AUTODYN was used to study the dynamic responses of the rock mass under varied blasting parameters, including the charge structure, initiation mode, and burden thickness. Finally, onsite experiments were carried out to demonstrate the vibration characteristics differences induced by different kinds of blastholes in the blasting excavation of the dam foundation.

2 Analysis of Blasting Parameters of Different Kinds of Blastholes in Dam Foundation Excavation

2.1 Definition of Blasting Parameters

Right after the detonation of the explosives, the detonation gaseous products with extremely high pressure and temperature fill the whole blasthole and act on blasthole wall, generating explosion shock waves. With the combination of gaseous products and shock waves, the rock around the blasthole yields and breaks, forming the crushing zone and the fracture zone (Esen et al. 2003; Shadabfar et al. 2021). The actions of shock waves and gaseous products on the rock mass are mainly affected by the explosion source; thus, these actions can be referred to as the inner blasting effects of explosives. The influencing factors associated to

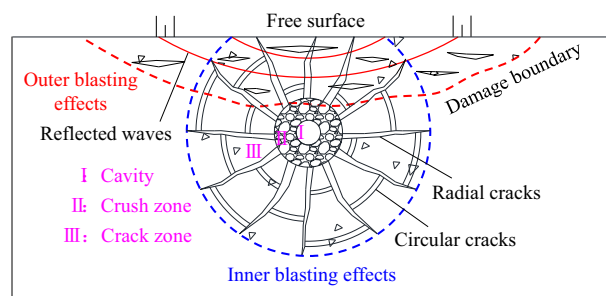


Fig. 1 Illustration of inner and outer blasting effects and partition of rock blasting fragmentation

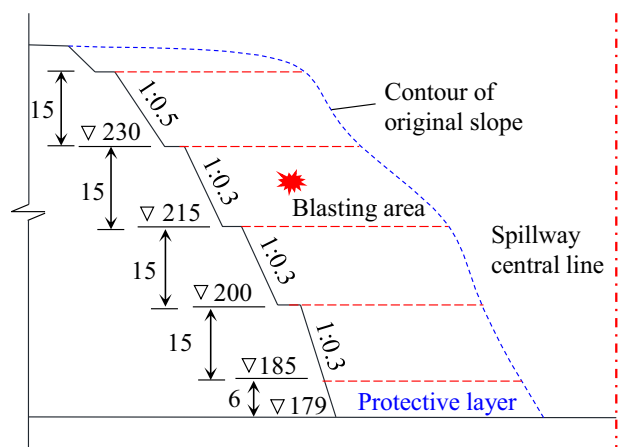


Fig. 2 Bench blasting in the excavation of rock slope

the explosive source, such as the charge structure, the initiation mode, and the blasthole spacing, can be classified as the inner blasting parameters. In addition, when compressive waves reach the free surface, reflected tensile waves are generated, causing spalling of the rock mass since its tensile strength is far lower than the compressive strength. The reflected waves are closely related to the free surfaces and the burden thicknesses, which are independent of the blasting sources; hence, the rock breakage by reflected waves can be defined as the outer blasting effects. Moreover, the burden thicknesses and the free surfaces can be categorized as the outer blasting parameters. Figure 1 shows the illustration of the inner and outer blasting effects.

2.2 Review of Blasting Methods in Dam Foundation Excavation

As the primary load-bearing structure for the hydropower station, the dam foundation is commonly excavated by bench blasting to control the blast-induced damage to reserved rock mass. As shown in Fig. 2, bench blasting excavation usually begins at the top of the rock slope, and the height of each

bench is approximately 8–15 m. At the bottom of the rock slope, a 3–6 m protective layer is reserved to protect the underlying rock foundation from blast-induced damage. For each bench of the rock slope, presplitting blasting or smooth blasting (as shown in Fig. 3) is adopted to guarantee the stability of the excavation profiles. In addition, to deal with the complex geological conditions of rock slope, several optimizations of blasting excavation based on presplitting blasting and smooth blasting were proposed during the construction of Baihetan Hydropower Station (Liu et al. 2020).

For the excavation of protective layer, not only should the blast-induced damage of the rock mass be controlled, but a flat blasting contour is also essential to reduce the over/underbreak. Over the past few decades, several effective excavation techniques for the excavation of protective layer were gradually developed. Those techniques include layered blasting excavation, horizontal presplitting blasting, horizontal smooth blasting, and bench blasting with bottom cushion-deck. To minimize blast-induced damage to the bedrock, the protective layer is usually divided into two or three thin layers in the layered blasting, and the height of the layer gradually decreases with the excavation of the protective layer. The layered blasting method is reliable for controlling bedrock damage, but the excavation procedures are complicated. To increase the efficiency of dam foundation excavation, the bench blasting with bottom cushion-deck method was proposed at Wan'an Hydropower Station in 1982 (Zhang et al. 2013). For the bench blasting with bottom cushion-deck method, a cushion deck comprised of various low-sonic-impedance materials is placed at the bottom of the blastholes to protect the bedrock by reducing the explosion energy transferred into the rock mass. However, the excavation profiles caused by bench blasting with bottom cushion-deck method can hardly meet the demands of practical engineering. Therefore, Lu et al. (2018) optimized the bench blasting with bottom cushion-deck method by placing the spherical energy-relief block on the bottom of the blastholes, and conducted several onsite experiments to verify the reliability of the optimized method in reducing blast-induced damage and controlling the shape of excavation profiles (Liu et al. 2020; Hu et al. 2020).

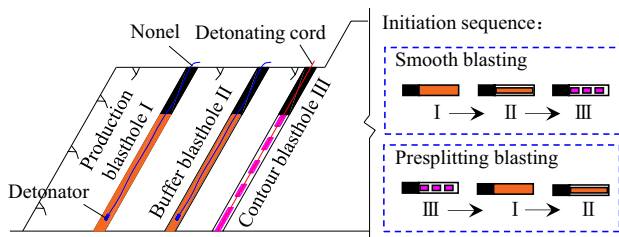


Fig. 3 Illustration of contour blasting of rock slope

The contour blasting techniques (horizontal presplitting blasting and horizontal smooth blasting) are widely used in the excavation of protective layer. To minimize the disturbance to the bedrock of the dam foundation, the contour blastholes and the buffering blastholes are drilled along the horizontal direction, while the production blastholes are arranged in the vertical or horizontal direction. For the contour blasting with vertical production blastholes, a pioneer slot used for placing drilling machine should be created in advance. So, the construction process is complicated restricting the excavation efficiency. The construction process of contour blasting with horizontal production blastholes is more concise, but it is hard to control the angle of horizontal drilling holes.

2.3 Differences in the Blasting Parameters of Different Kinds of Typical Blastholes

As stated above, three typical types of blastholes, including presplitting blasthole, smooth blasthole, and production blastholes are widely adopted in different kinds of blasting methods in dam foundation excavation. In addition, their blasting parameters are of significant differences due to their own roles in rock blasting.

2.3.1 Inner Blasting Parameters

(1) Charge Structures

To minimize the blast-induced damage to the surrounding rock mass, explosives in contour blastholes are axially and radially decoupled from the rock mass (i.e., presplitting blastholes and smooth blastholes). Unlike contour blastholes, explosives in production blastholes are continuous in the axial direction, and the decoupling ratio in the radial direction is substantially lower than that in the contour blastholes. Therefore, the blasting pressure on the hole wall of contour blasthole is smaller than that of production blasthole since there are more uncoupled mediums, such as air and water, etc. The differences in charge structures of different kinds of blastholes are shown in Fig. 4.

(2) Initiation modes

As the explosives in contour blastholes are axially decoupled from the rock mass, the detonating cord is always adopted to guarantee the reliable detonation of each explosives segment. The detonation velocity of the detonating cord is much higher than that of commercial explosives. Thus, the explosives in the contour blastholes are approximate to lateral detonation, and the detonation wave propagates along the radial direction of the blasthole. The explosives in production blastholes are fired by detonators, so the detonation wave propagates axially along the blasthole from the site of

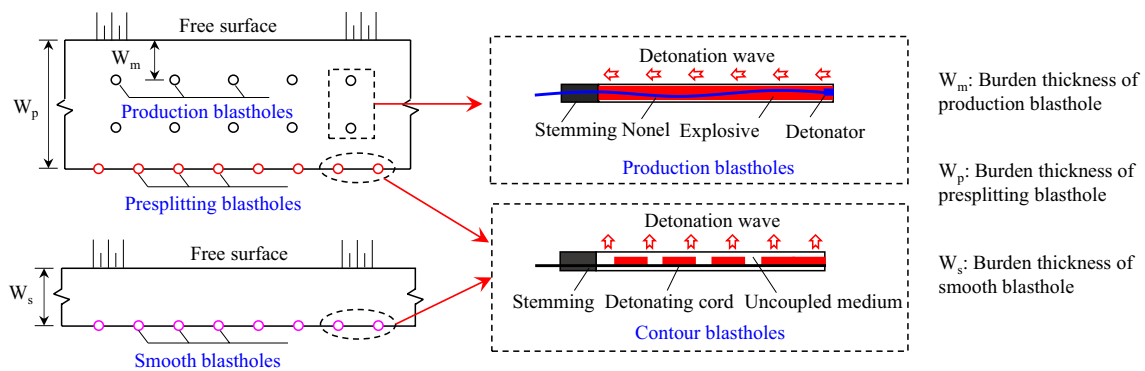


Fig. 4 Differences in blasting parameters of various blastholes in dam foundation excavation

initiation. For different initiation modes, the detonation processes of explosives in cylinder blastholes are different, further affecting the blasting pressure on the hole wall and inner blasting effects. Figure 4 illustrates the propagation directions of detonation waves under different initiation modes.

2.3.2 Outer Blasting Parameters

As illustrated in Fig. 4, to isolate the blast vibration induced by production blastholes, the presplitting blastholes are usually fired at the first row. So, the burden thicknesses of presplitting blastholes are significantly greater than those of production blastholes. Nevertheless, with the increase of burden thicknesses, the clamping force of the blasthole gradually increases, which further reduces the outer blasting effects. Since smooth blastholes are usually initiated after other blastholes to generate a flatter excavation profile, the burden thicknesses are relatively small, hence enhancing the outer blasting effects.

3 Effects of Blasting Parameters on Blasting Vibration Responses

3.1 Theoretical Analysis

3.1.1 Distribution of Explosion Energy

The explosion energy can be divided into four parts: the fragmentation energy, the seismic energy, the kinetic energy used for the displacement of blast-induced fragments, and other energy transferred in a less apparent way, such as the energy used for plastic and elastic deformation of rock masses, and the energy transferred into the rock mass from the hot detonation products (Sanchidrián et al. 2007). Under different inner and outer blasting parameters, the explosion energy components are different. For example, when the

explosives in blastholes are decoupled from the rock mass, the detonation pressure on the blasthole wall decreases as the radius of the decoupled medium (e.g., air and water) increases, hence reducing the radius of the plastic zone and weakening the inner blasting effects. This means that more proportions of explosion energy will convert into seismic energy.

During the detonation of the explosives in blasthole, there is always an unsteady detonation zone that extends 3–6 times the diameter of the blasthole before the detonation shock waves reach steady-state velocities. This unsteady detonation zone is known as the run-up distance (Leng et al. 2016). When explosives are laterally initiated by the detonating cord, the actual detonation velocity of the main explosives in contour blastholes is lower than their steady-state velocity as the existence of the run-up distance. The run-up distance also exists in the end initiation by the detonator, but it is much smaller than the length of the explosive column. Therefore, it can be assumed that under the end initiation, the explosives in the blasthole are detonated in a steady-state velocity (Leng et al. 2016). According to the C-J (Chapman-Jouguet) detonation theory, the correlation between detonation pressure and detonation velocity is positive (Chapman 1899). Consequently, under side initiation, the detonation pressure on the blasthole wall and the inner blasting effects are relatively weaker, resulting in a greater conversion of explosion energy to vibration energy.

Moreover, the outer blasting parameters, including the burden thicknesses and the numbers of free surfaces, also have a substantial effect on the distribution of explosion energy. After the initiation of explosives, the blast-induced shock waves attenuate rapidly in rock masses. As the burden thickness increases, the intensity of the tensile stress waves reflected from the free surface gradually decreases, and less explosion energy is converted into fragment energy, resulting in more large size fragments, which is disadvantageous to the downstream blasting operation (An et al. 2018). The numbers of free surfaces are also closely related to the generation of the

reflected tensile waves. Increasing the number of free surfaces means that there are more excitation sources for reflected tensile stress waves, which is helpful for weakening the clamping force of the blastholes and increasing the consumption levels of explosion energy for rock fragmentation and displacement.

3.1.2 Influences of the Plastic Zone on Dominant Frequency

The frequency spectrum of blasting vibration is complex, and a variety of parameters, such as charge weight per delay, longitudinal wave velocity, density of rock mass, radius of the elastic zone, and distance from the blasting sources, all have influences on the distribution of the dominant frequency. Based on those parameters, Lu et al. (2015) proposed a prediction equation describing the attenuation of the dominant frequency against the distance from the blasting sources.

$$f = \xi \frac{C_p}{Q_0^{1/2}} \left(\frac{Q_0^{1/2}}{r} \right)^\beta \quad (1)$$

$$Q_0 = \frac{4}{3} \pi q a_0^3 \quad (2)$$

where f is the dominant frequency, ξ and β are the on-site coefficients related to the geological condition, C_p is the longitudinal wave velocity of the rock mass, Q_0 is the quality of the explosives, r is the distance from the blasting source, q is the density of the rock mass, and a_0 is the radius of the plastic zone.

Lu et al. (2015) fitted the prediction equation based on the onsite experiment, and the results indicated that the dominant frequency of onsite blasting vibration is inversely proportional to the radius of the plastic zone. Moreover, the average frequency, which is described by Eq. (3), was used to investigate the influences of the plastic zone. The research results also showed that as the radius of the plastic zone increases, the average frequency gradually decreases.

$$\bar{f} = \frac{\sum f_i A(f_i)}{\sum A(f_i)} \quad (3)$$

where \bar{f} is the average frequency, f_i is the individual frequency in the Fourier amplitude spectrum and $A(f_i)$ is the amplitude of each frequency f_i .

3.2 Numerical Simulation Analysis

From the analysis of the blasting parameters in Sect. 3.1, it is obvious that variations in these parameters will affect the dynamic response of rock mass, leading to discrepancies in blasting vibration characteristics. For various typical blastholes in the excavation of a dam foundation, the differences in their blasting parameters concentrate on the charge structure, initiation mode and burden thickness. Therefore, to figure out the inherent causes of the vibration characteristics differences induced by different kinds of blastholes, numerical models for investigating the dynamic response of the rock mass were established in relation to the above-mentioned blasting parameters.

3.2.1 Numerical Models

The RHT (Riedel–Hiermaier–Thoma) material model developed by Riedel et al. (1999) was used for the rock materials in the numerical simulation. Based on the HJC (Holmquist–Johnson–Cook) material model, the RHT model adds the failure surface, elastic limit surface, and remaining strength surface to describe the variation of initial yield strength, failure intensity, and residual strength. Moreover, the influences of pressure hardening, strain hardening, and third invariant dependence on the damage of the rock mass are considered comprehensively in the RHT model. The failure surface equation of the RHT model is expressed as follows:

$$\begin{cases} \sigma_{\text{eq}}^*(P, \theta, \dot{\epsilon}) = Y_{\text{TXC}}^*(P) R_3(\theta) F_{\text{rate}}(\dot{\epsilon}) \\ Y_{\text{TXC}}^*(P) = A(P^* - P_{\text{spall}}^* F_{\text{rate}}(\dot{\epsilon}))^N \\ P_{\text{spall}}^* = P_{\text{spall}}/f_c \end{cases} \quad (4)$$

where P is the pressure, θ and $\dot{\epsilon}$ are the Lode angle and strain rate, respectively, $Y_{\text{TXC}}^*(P)$ is the equivalent stress intensity on compression, $R_3(\theta)$ is the angular even function on a partial plane, P^* is the pressure normalized by f_c , $F_{\text{rate}}(\dot{\epsilon})$ is the strengthening factor of the strain rate, P_{spall}^* is the spall strength normalized by f_c , P_{spall} is the spall strength, A is the constant of the complete failure surface, N is an index of the complete failure surface, and f_c is the uniaxial compressive strength.

Furthermore, based on the Holmquist and Johnson constitutive models, the damage variable D is introduced to describe the residual failure surface, and the damage is assumed to be

the accumulation of inelastic strain (Wang and Zhang 2014), which is expressed as follows:

$$\begin{cases} D = \sum \frac{\Delta \epsilon_p}{\epsilon_p^{failure}} \\ \epsilon_p^{failure} = D_1(P^* - P_{*spall})^{D_2} \geq \epsilon_f^{min} \end{cases} \quad (5)$$

where D_1 and D_2 are the damage constants for describing the strain effect, $\epsilon_p^{failure}$ is the failure strain, ϵ_f^{min} is the minimum strain to reach failure, and $\Delta \epsilon_p$ is the plastic strain variation. Table 1 shows the detailed mechanical parameters of the rock mass used for the numerical models (Xie et al. 2017).

To describe the expansion processes of the detonation products, the JWL (Jones-Wilkins-Lee) equation of state (Lee et al. 1968) was adopted, and the relationship between the pressure of detonation products, volumes, and energy can be expressed by Eq. (6).

$$P_d = A_1 \left(1 - \frac{\omega}{R_1 V} \right) e^{-R_1 V} + B_1 \left(1 - \frac{\omega}{R_2 V} \right) e^{-R_2 V} + \frac{\omega E}{V} \quad (6)$$

where P_d is the pressure of detonation products, V is the relative volume of detonation products, E is the detonation energy per unit volume, and $A_1, B_1, R_1, R_2,$ and ω are independent parameters defined by the properties of explosives.

Table 2 lists the related parameters of the explosives (Xie et al. 2017).

Based on the experiment conducted by Banadaki and Mohanty (2012), another numerical model for demonstrating the reliability of the numerical parameters was established by ANSYS AUTODYN. Similar to the results of the laboratory experiment, the cracks simulated in numerical model extend uniformly from the center of the blasthole, generating the crush zone and the crack zone around the blasthole. The radius of the simulated crush zone is approximately 4.5 times that of the blasthole, while that of the laboratory experiment is 5–6 times that of the blasthole, which demonstrates the feasibility of both the numerical parameters and the numerical models.

3.2.2 Analysis of the Effect of Decoupling Ratios

To investigate the dynamic response of the rock mass under different charge structures, plane strain models measuring 5 m × 5 m were implemented. As shown in Fig. 5, since the production blastholes are usually initiated individually by the detonator, a single blasthole with a diameter of 90 mm was arranged in the center of the numerical model. The diameters of the explosives in the production blastholes were set as 70 mm, and the decoupling ratios were 1.3. For contour blastholes (i.e., smooth blastholes and presplitting blastholes), three or four blastholes with larger decoupling ratios are typically initiated at one shot by the detonator cord. Therefore, four blastholes with decoupling ratio of 2.6

Table 1 Parameters used in the RHT model for rock materials

ρ (g·cm ⁻³)	G (GPa)	f_c (MPa)	D_1	D_2	A	N
2.75	16.7	35	0.04	1.0	1.6	0.61

Table 2 Parameters of the explosives

ρ (kg·m ⁻³)	VoD (m·s ⁻¹)	P_{d0} (GPa)	A_1 (GPa)	B_1 (GPa)	R_1	R_2	ω
1000	5000	5.15	49.4	1.89	3.9	1.11	0.33

Fig. 5 Numerical models: **a** numerical model of a production blasthole with decoupling ratios of 1.3 and **b** numerical model of contour blastholes with decoupling ratios of 2.6

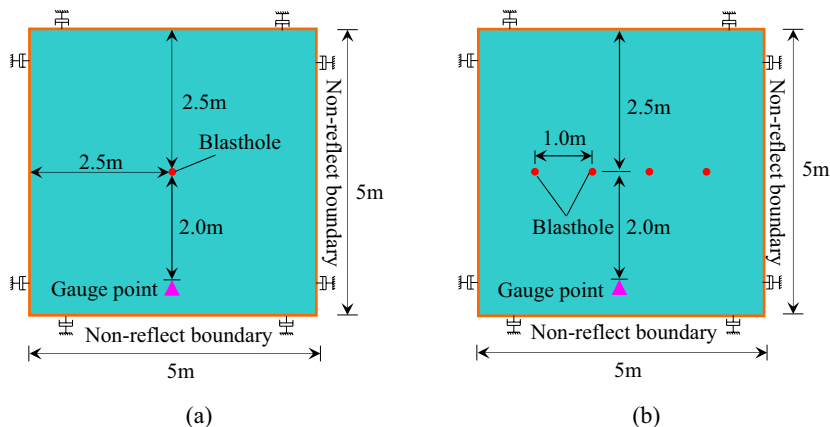
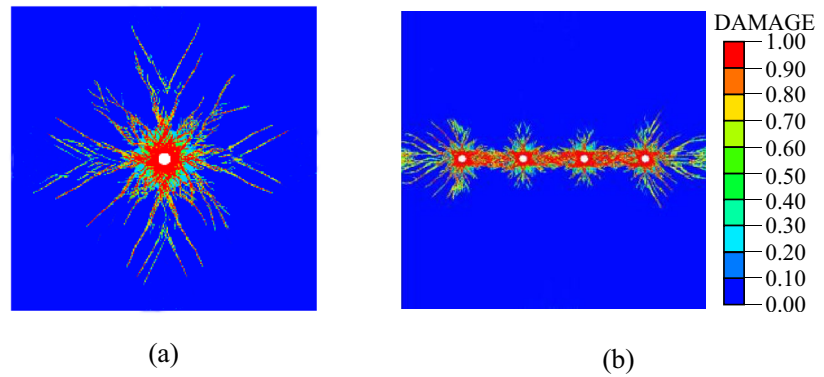


Fig. 6 Results of blast-induced damage under different decoupling ratios: **a** decoupling ratio 1.3 and **b** decoupling ratio 2.6



were arranged in the model to maintain identical amounts of explosive quantity at one shot for each blasthole type. The diameters of the contour blastholes were set as 90 mm, and the diameters of the explosives inside were set as 35 mm. In addition, for each model, a gauge point was arranged 2.0 m below the blastholes to extract and calculate the blasting vibration energy.

To eliminate the artificial wave reflections from reentering the model, the transmit boundaries were enforced on all surfaces. The explosive and rock mass were modeled using Eulerian elements and Lagrangian elements, respectively, and all the elements had dimensions of 5 mm × 5 mm. Moreover, fluid–structure interaction was adopted in the numerical models, and the air was used as a coupling medium between the RHT material and the explosives.

The results of blast-induced damage under different decoupling ratios are shown in Fig. 6. For the single blasthole with a decoupling ratio of 1.3, blast-induced damage and the cracks around the blasthole spread uniformly from the center of the blasthole outward. When the decoupling ratio increase to 2.6, a through crack is formed between the adjacent holes; however, the extents of blast-induced damage and cracks is significantly decreased. Increasing the decoupling ratio means a thicker air interlayer between the explosives and the blasthole wall, weakening the blasting pressure on the blasthole wall and inner blasting effects which further led to a reduction in the blast-induced damage and the radius of the plastic zone. Figure 7 shows the blasting pressure curves on the blasthole wall. As shown in this figure, the durations of the blasting pressure are similar under different charge structures, but the peak values are notably distinct. In the case of the decoupling ratio of 1.3, the peak value of the blasting pressure is approximately 1.21 GPa, which is obviously higher than that under the decoupling ratio of 2.6.

To study the explosion energy distribution under different charge structures, the time–energy curves of the measuring points in Fig. 5 were calculated by time–energy density analysis based on the wavelet transform (Lu et al. 2018). Noting that the quality of explosives for different decoupling ratios were equal. Consequently, the total

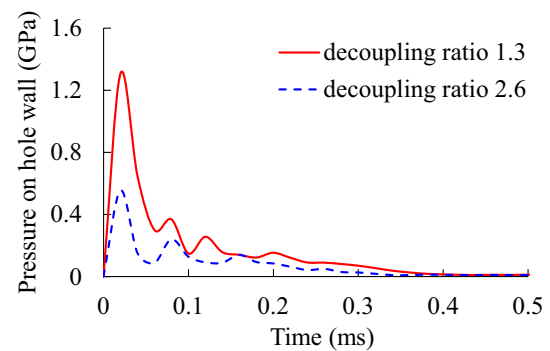


Fig. 7 Blasting pressure curves under different decoupling ratios

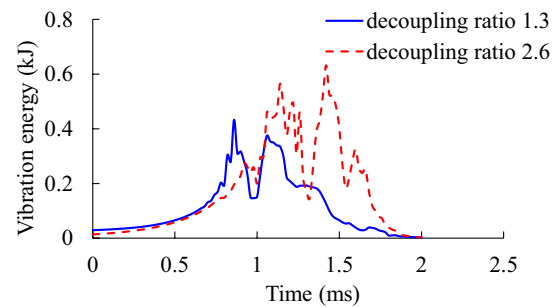


Fig. 8 Time-energy curves under different decoupling ratios

amount of explosion energy released under various decoupling ratios is at the same level. The results are shown in Fig. 8. As illustrated, the peak value of the time–energy curve under the decoupling ratio of 2.6 is 0.61 kJ, which is significantly higher than that under the decoupling ratio of 1.3. When the maximum charge of each shot and the distances from the explosion sources are at the same level, more proportion of explosion energy is converted into vibration energy as the decoupling coefficient increased.

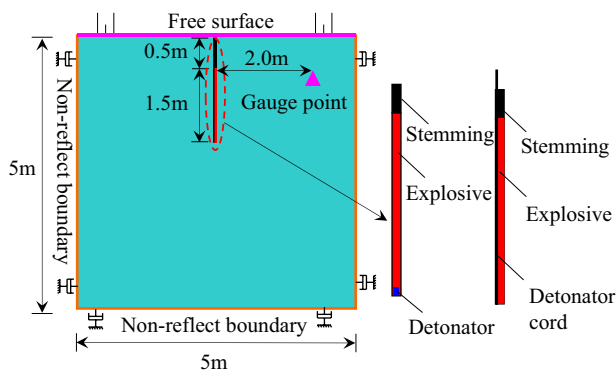


Fig. 9 Numerical models under different initiation modes

3.2.3 Analysis of the Effect of Initiation Modes

As stated above, the distribution of explosion energy is different under various initiation modes. To study the influences of different initiation modes on the dynamic response of the rock mass, axisymmetric plane numerical models measuring 5 m × 5 m were conducted. As shown in Fig. 9, the length of the blasthole is 2.0 m, and the diameter is 90 mm. Free boundaries were selected for the top surfaces of the models, while the transmit boundaries were enforced for the remaining surfaces to avoid the artificial wave reflections generated at the boundaries reentering the model. Moreover, the Lee-Tarver model (Lee and Tarver 1980), expressed in Eq. (7) was used for the explosives under lateral initiation to describe the nonideal detonation process. The parameters of the Lee-Tarver model are provided in Table 3.

$$\begin{cases} \frac{\partial F}{\partial t} = I \cdot (1 - F)^b \cdot (\mu - a)^x + G_1 \cdot (1 - F)^c \cdot F^d \cdot P_0^y + G_2 \cdot (1 - F)^e \cdot F^g \cdot P_0^z \\ \mu = \frac{V_3}{V_4} - 1 \end{cases} \quad (7)$$

Table 3 Parameters of the Lee-Tarver model

$I (\mu s^{-1})$	a	b	c	d	e	g	x	y	z	$G_1 (Mbar^{-y} \cdot \mu s^{-1})$	$G_2 (Mbar^{-y} \cdot \mu s^{-1})$
50	3.712	0.032	0	0	0.22	0.66	4	0	1.2	0	40

where P_0 is the pressure in the explosive, F is the reaction ratio, t is time, μ is the compression ratio, V_3 is the initial specific volume of the explosive, V_4 is the specific volume of the shocked and unreacted explosive, and $I, b, a, x, G_1, c, d, y, G_2, e, g,$ and z are constants.

When explosives are initiated by the detonator at one end of the blasthole, the explosion energy tends to gather toward the non-initiation side (Gao et al. 2019b). So, as shown in Fig. 10 (a), the damage radius at the top end is much larger than that at the bottom end, and the blast-induced damage of the rock mass around the blasthole appears to be in the shape of an inverted triangle. Unlike end initiation, when the explosives are laterally initiated by the detonation cord, the detonation wave mainly propagates along the radial direction of the blasthole. Therefore, as shown in Fig. 10(b), the damage contour under lateral initiation is uniformly distributed along the axial direction. Moreover, the equivalent damage radius under end initiation is much larger than that under lateral initiation. Figure 11 gives the blasting pressure curves on the bottom, middle, and top of the blasthole wall under different initiation modes. For the end initiation, the start raising time and peak value of the blasting pressure at different locations of the blasthole wall are different, since the time and directional effects along the charge are different. However, under lateral initiation, the blasting pressure curves at different locations of the blasthole wall are similar, and their peak values are approximately 0.8 GPa, which is much smaller than the peak values of the pressure on the top of the blasthole wall under end initiation. Therefore, the inner blasting effects under end initiation are significantly stronger than that under lateral initiation.

Fig. 10 Results of blast-induced damage under different initiation modes: a end initiation and b lateral initiation

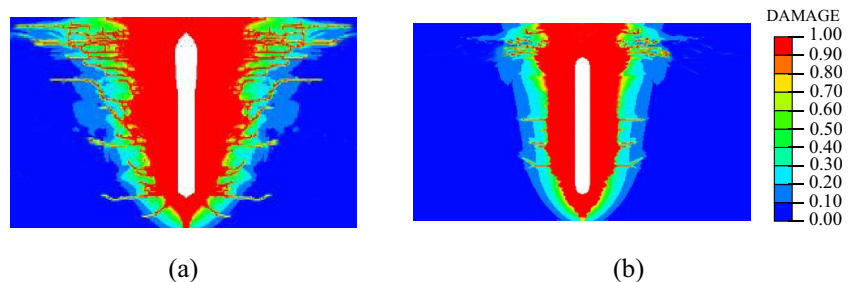


Fig. 11 Blasting pressure curves under different initiation modes: **a** end initiation and **b** lateral initiation

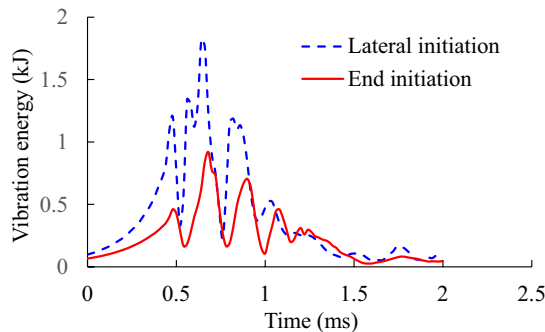
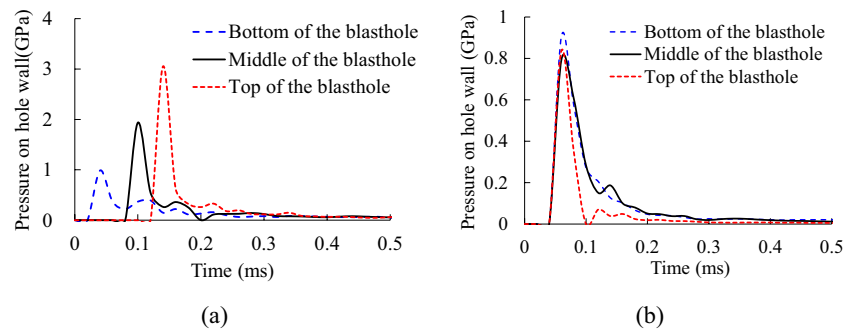


Fig. 12 Time-energy curves under different initiation modes

To extract and calculate the blasting vibration energy, a gauge point was arranged at 2 m to the right side of the blasthole, and the time–energy curves for different initiation modes are provided in Fig. 12. As illustrated, the peak value of the time–energy curve for lateral initiation is 1.82 kJ, which is significantly greater than 0.92 kJ for end initiation. After the detonation of the explosives, there is a run-up distance of approximately 3–6 times the diameter of the blasthole before the detonation shock wave arrives at a steady-state velocity. Therefore, the actual detonation velocity under lateral initiation is lower than the inherent detonation velocity, and the initiation reaction of explosives can be regarded as a non-ideal detonation process, resulting in the reduction of the detonation pressure on the blasthole wall and the radius of the blast-induced damage zone. As a result, the proportion of explosion energy used for fragmentation and displacement decreases, and more explosion energy is converted into seismic energy.

3.2.4 Analysis of the Effect of Burden Thicknesses

It is a common belief that the variations in burden thickness change the clamping forces of blastholes, thereby influencing the dynamic responses of the rock mass (Sanchidrián et al. 2007). To investigate the influences of the burden thicknesses, three plain strain models with burden thickness of 2.0 m, 1.5 m, and 1.0 m, respectively, were developed. As shown in Fig. 13, all of these models were built using

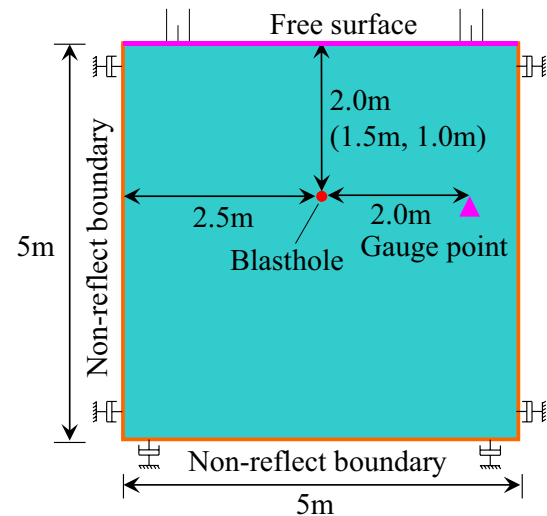


Fig. 13 Numerical models under different burden thicknesses

quadrilateral elements with an 5 mm × 5 mm element size. To prevent wave-reflecting effects, transmit boundaries were applied on all surfaces, excluding the top surface. Moreover, a gauge point was arranged at 2.0 m on the right side of the blasthole to extract and calculate the blasting vibration energy under different burden thicknesses.

Figure 14 illustrates the results of blast-induced damage under different burden thicknesses. As shown in this figure, the damage intensity of the rock mass in front of the blasthole increases gradually as the burden thicknesses decreases. The reduction in the burden thickness enhances the reflected waves from the free surface, causing intense spalling of the rock mass around the free surface. To analyze the explosion energy distribution under different burden thicknesses, the time–energy curves of the gauge point were analyzed, and the results are provided in Fig. 15. As illustrated, the vibration energy arrives at a peak value at 1.1 ms, and reduces as the burden thickness decreases. This is due to the fact that the reduction of burden thickness weakens the clamping force on the blasthole, and enhances the outer blasting effect and the intensity of the reflected waves generated at

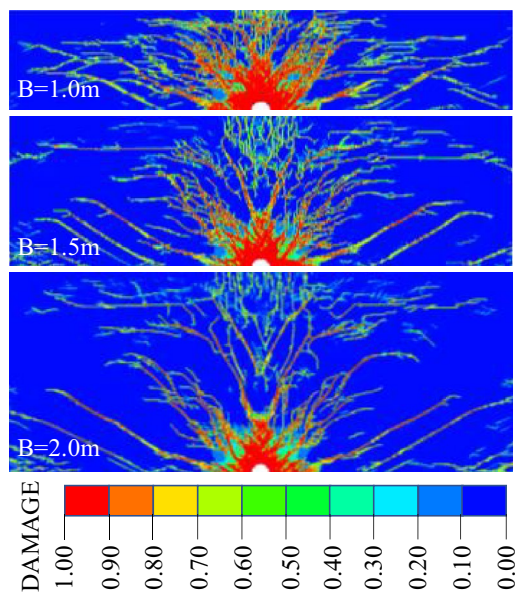


Fig. 14 Results of blast-induced damage under different burden thicknesses

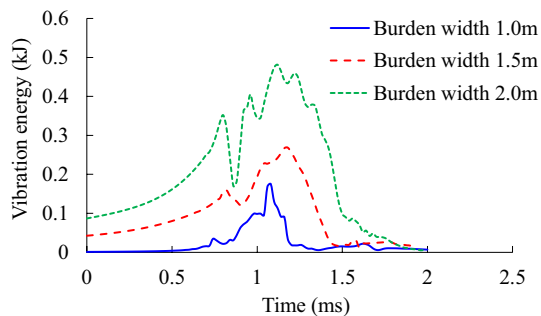


Fig. 15 Time-energy curves under different burden thicknesses

the free surface, resulting in a greater consumption of explosion energy for rock fragmentation and displacement.

4 Case Study

4.1 Site Description

The Baihetan Hydropower Station is located downstream of the Jinsha River, a branch of the Yangtze River in Sichuan and Yunnan Province in southwest China. The station has 16 turbines, each with a generating capacity of 1.0 GW. In terms of generating capacity, Baihetan Hydropower Station is the second largest hydropower station in China, after the Three Gorges Hydropower Station. The bedrock of the dam foundation is composed of weakly weathered breccia lava, with compressive strengths ranging from 55 to 70 MPa.

Figure 16 shows the location of the Baihetan Hydropower Station and the experimental sites.

4.2 Blasting Design and Vibration Monitoring

To investigate the vibration characteristics induced by different kinds of blastholes, a horizontal presplitting blasting experiment and a horizontal smooth blasting experiment were conducted in the excavation of the horizontal section of the dam foundation. The layout of the onsite blasting experiments is shown in Fig. 16. For different blasting experiments, the arrangements of blastholes were similar, including both the vertical production blastholes and horizontal contour blastholes. Figure 17 illustrates the initiation network in the onsite experiments. As shown, in the horizontal smooth blasting experiment, the vertical production blastholes were fired first to separate the blasting vibration of production blastholes from that of smooth blastholes. Then, the blast-induced rock slugs were removed via high-pressure water or air, and the smooth blastholes were detonated. Table 4 shows a list of the detailed drilling and blasting parameters, and Fig. 18 shows a plot of the typical charge structures of production blastholes and contour blastholes. In addition, non-electric millisecond detonators MS2, MS3, and MS5 were adopted to fire various rounds of production blastholes, while MS5 and MS3 were used for contour blastholes. To separate the blast vibration of the first two production blastholes from the others, MS9 was adopted inside the blue production blastholes in Fig. 17, and MS11 was adopted inside the rest of the production blastholes.

To record the vibration induced by different kinds of blastholes, the monitoring holes marked in Fig. 17 were drilled before each blasting experiment. The vertical vibration sensors CDJ28 made by the Chongqing Geological Instrument Factory, China, were installed in the monitoring holes, and they were placed at 1.0 m, 1.5 m, and 2.0 m below the foundation surface. Figure 19 shows the locations of the monitoring points.

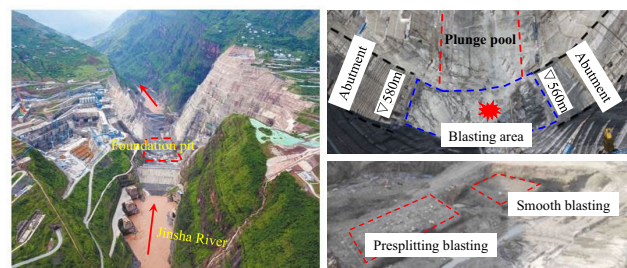


Fig. 16 Layout of the blasting experiment sites at the Baihetan Hydropower Station

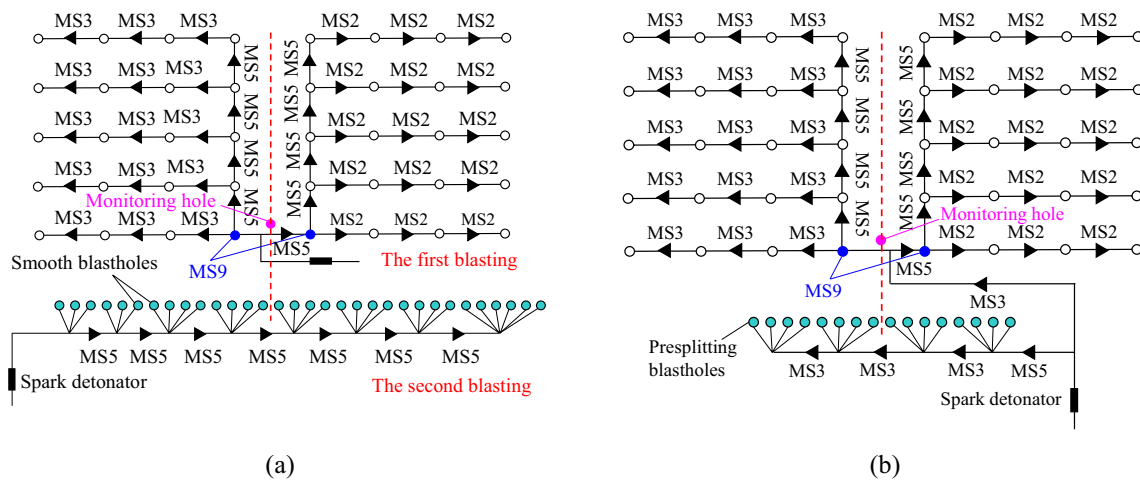


Fig. 17 Initiation networks: **a** horizontal smooth blasting experiment and **b** horizontal presplitting blasting experiment

Table 4 Drilling and blasting parameters

Blasthole type	Hole diameter (mm)	Hole depth (m)	Stemming (m)	Charge weight (kg)	Charge diameter (mm)	Charge weight at one shot (kg)
Presplitting blasthole	76	10	1	2.2	32	8.8
Smooth blasthole	76	10	1	2.2	32	8.8
Production blasthole	90	3.5	1.5	4.3	70	4.3

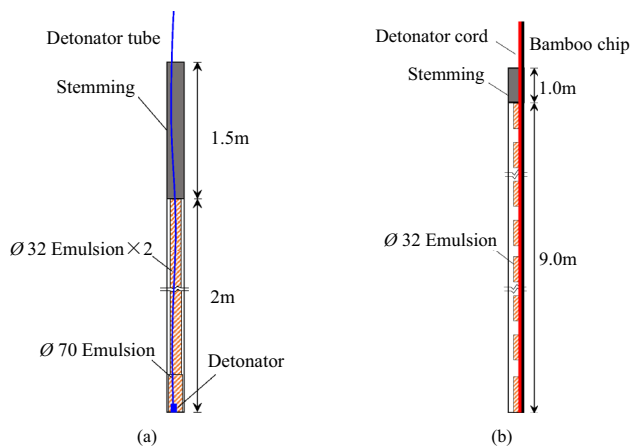


Fig. 18 Typical charge structures: **a** production blasthole and **b** contour blasthole

4.3 Results Analysis

In presplitting blasting experiment, the presplitting blastholes were fired before the production blastholes. Consequently, the vibration signal transmission line in the monitoring holes was destroyed by the flying rock debris, resulting in the loss of the vibration signal of the production

blastholes. In smooth blasting experiment, the production blastholes were detonated at first stage, then the blast-induced rock slags were removed via high-pressure water or air. Finally, the smooth blastholes were fired to generate flat excavation profiles. So, the vibration signals of both smooth blastholes and production blastholes were recorded by the vibration sensors during the smooth blasting experiment. The typical blasting vibration waveforms of measuring point #1 are shown in Fig. 20. As illustrated in Fig. 21, the PPVs induced by smooth blastholes and production blastholes were approximately equivalent, 14.6 cm/s and 13.8 cm/s, respectively, which were smaller than the PPVs induced by presplitting blastholes.

In practice, there are always 3–4 contour blastholes (i.e., presplitting blastholes and smooth blastholes) initiated at the same time per delay; thus, the maximum charge of each shot of contour blastholes is significantly higher than that of production blastholes. As shown in Table 4, the maximum charge per delay of the contour blastholes is 8.8 kg, while that of the production blasthole is 4.4 kg. To avoid the influences of the maximum charge of each shot, the Sadovsky formula (Zeng et al. 2018) was adopted to analyze the vibration characteristics induced by different kinds of blastholes. The equation has the following forms:

Fig. 19 Layout of the monitoring holes: **a** contour blastholes blasting and **b** production blastholes blasting

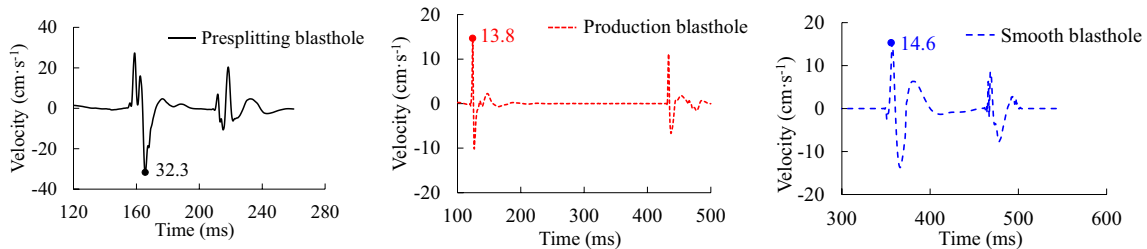
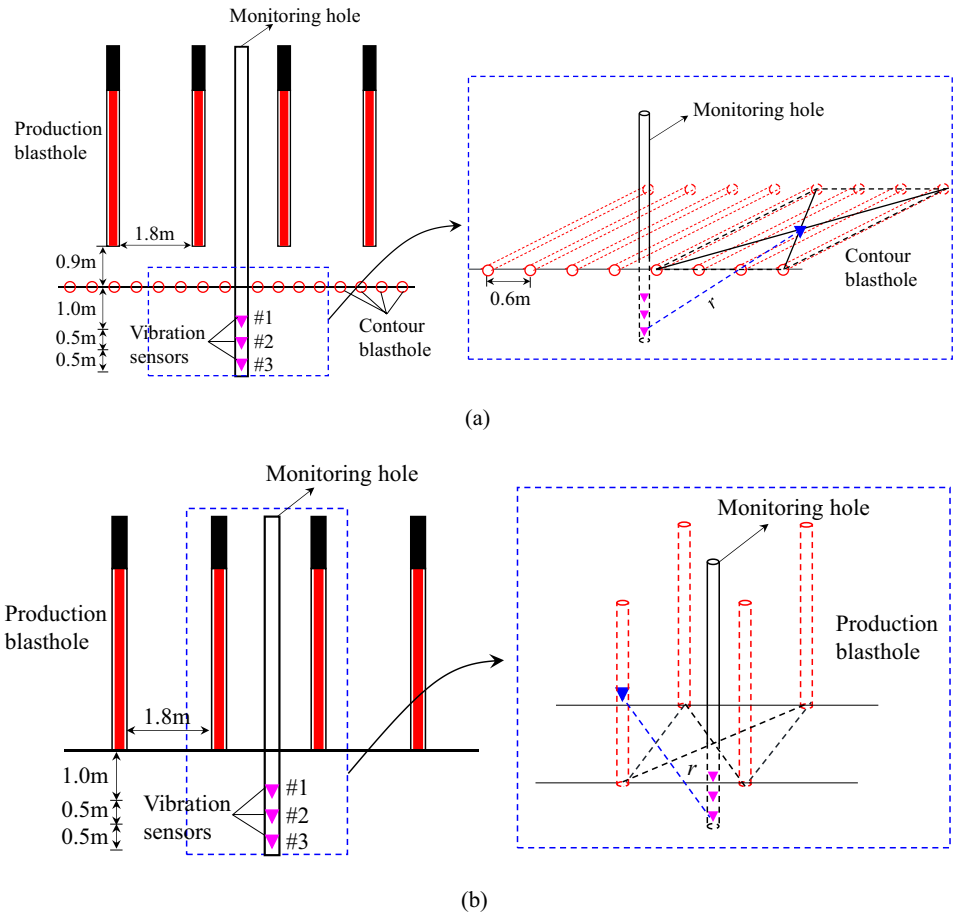


Fig. 20 Measured velocity–time histories induced by different kinds of blastholes at both measuring points #1

$$PPV = K(SD)^{-\alpha} \tag{8}$$

$$SD = r/Q^{1/3} \tag{9}$$

where K and α are factors related to the onsite geological conditions, r is the distance from the explosion center, and Q is the maximum charge per delay. As shown in Fig. 17, the recorded production blastholes were isolated by MS9, so the r for production blastholes was defined as the distance from the monitoring point to the center of the charge (see Fig. 19b). Unlike production blastholes, the r for contour blastholes was defined as the distance from the monitoring

point to the center of the contour blastholes per delay since 3–4 contour blastholes are usually initiated at the same time (see Fig. 19a). The fitting results of the PPV against SD curves are provided in Fig. 21. As illustrated, the PPVs induced by presplitting blastholes are larger than those induced by smooth blastholes and production blastholes, while the PPVs induced by smooth blastholes and production blastholes are approximately at the same level.

Moreover, the amplitude–frequency spectrum $F(\omega)$, available from Fourier transformation, was normalized for better comparison, and the results are provided in Fig. 22. As illustrated, the amplitude–frequency spectra of presplitting blastholes have complex structures of double or triple

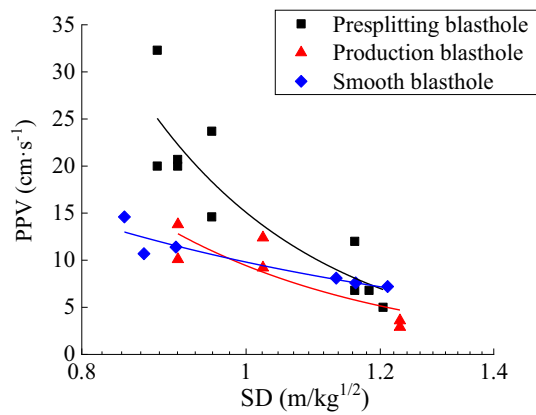


Fig. 21 PPV against SD curves of different kinds of blastholes

peak values. Unlike the presplitting blastholes, the amplitude–frequency spectra of smooth blastholes and production blastholes are dominated by a single peak. Furthermore, the dominant frequencies of presplitting blastholes are concentrated in 50–100 Hz, which is much higher than smooth blastholes and production blastholes.

To analyze the energy distribution against the frequency, the vibration signals were decomposed into 11 frequency bands (d_1 to d_{11}) by the wavelet basis function *sym8*. Then, the decomposed signals were reconstructed by the *Wcoef* function (Zhong et al. 2008). Taking measurement point #1 as an example, the reconstructed signals of blasting vibration waveforms induced by presplitting blastholes are shown in Fig. 23. As illustrated, the spectrum of the vibration signal in the first layer ranges from 4000 to 8000 Hz, and the spectral range decreases by a factor of two with each decomposition. Furthermore, the vibration energy of each layer was calculated by the following equation (Ma et al. 2022):

$$E_i = \sum_{n=1}^M |d_i(n)|^2 \quad i = 1, 2, \dots, Z \quad (10)$$

$$E_0 = \sum_{i=0}^M |a_N(n)|^2 \quad (11)$$

$$E_t = \sum_{i=0}^N \int_{-\infty}^{+\infty} g_i^2(t) dt = \sum_{i=0}^Z E_i \quad (12)$$

$$\varepsilon_i = \left(\frac{E_i}{E_t} \right) \times 100\% \quad (13)$$

where E_i is the frequency band energy of each component of vibration signal, M is the number of sampling points, Z is the number of decomposed layers, $a_N(n)$ is the approximation coefficient of the decomposed layer Z , and $d_i(n)$ is the detail coefficient of the decomposed layer i , E_t is the total energy of vibration signal, $g_i(t)$ is the vibration signal in high frequency, ε_i is the proportion of energy in each frequency band to the total energy.

Figure 24 presents the energy distribution against frequency bands at each monitoring point. For the presplitting blastholes, the vibration energy was concentrated in frequency band *d7* (62.5 Hz to 125 Hz). Similar to Fig. 22, the presplitting blastholes dominant frequency band is higher than those of smooth blastholes and production blastholes at each point.

5 Discussion

In previous studies, it has been generally accepted that the presplitting cracks, the explosive quality at one shot, and the distance from the explosion center (Singh et al. 2014; Torano et al. 2006; Yilmaz and Unlu 2013) determine the vibration characteristics differences of various blastholes, ignoring the influences of the blasting parameters to some degree. However, in the present study, the horizontal smooth blasting experiment and the horizontal presplitting blasting experiment were conducted to avoid the influences of the pre-splitting cracks. Furthermore, to avoid the influences of

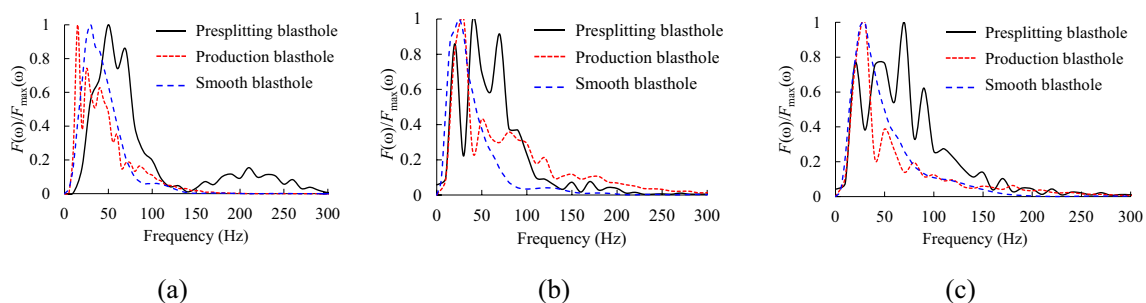


Fig. 22 Comparison of the amplitude–frequency spectra of vibration signals induced by different kinds of blastholes: **a** measurement point #1, **b** measurement point #2 and **c** measurement point #3

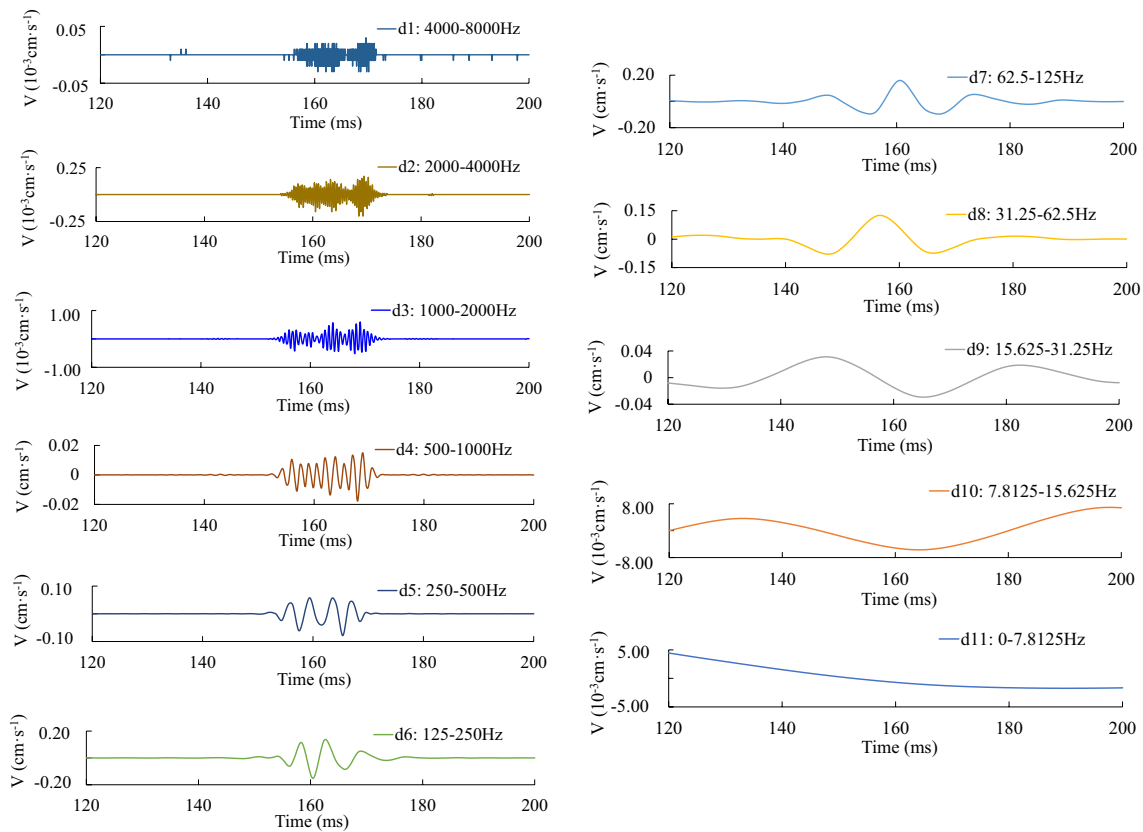


Fig. 23 Components of blasting vibration induced by presplitting blast-holes at measurement point #1

the distance from explosion sources and the quality of the explosives, the Sadovsky formula (Zeng et al. 2018) was adopted in the analysis of the vibration induced by different kinds of blastholes. Obviously, only in the case of different blasting parameters, the experimental results (Fig. 21 and Fig. 22) show that the PPVs and dominant frequencies induced by presplitting blastholes are much higher than those of the smooth blastholes and production blastholes, which are both almost at the same level.

In addition to the above-mentioned factors, the blasting parameters may also affect the explosion energy distribution and the evolution of the plastic zone, thereby contributing to the differences in vibration characteristics induced by different kinds of blastholes. For presplitting blastholes, they are laterally initiated by the detonation cord at the first blast row, and the explosives are generally radially and axially decoupled from the rock mass. Therefore, the inner and outer blasting effects of presplitting blastholes are relatively weaker. More explosion energy is dissipated in the form of blasting vibration, causing a reduction in the radius of the plastic zone. In addition, the charge structures and initiation modes of smooth blastholes are similar to those of presplitting blastholes, but their burden thicknesses are smaller, which increases the outer blasting effects of blastholes. The

explosives in production blastholes are always initiated by the detonator at the end of the blasthole, and their decoupling ratios are smaller than those of contour blastholes, resulting in a stronger inner blasting effect. Nevertheless, the burden thicknesses of smooth blastholes are smaller than those of production blastholes, so the vibration energy conversion and the plastic zone development of smooth blastholes and production blastholes are approximately at the same level due to the balance of their inner and outer blasting effects.

As known to all, the damage mechanisms of structures vary with the distance from the explosion source in rock blasting. For example, when the structures are located in the vicinity of the explosion sources, the PPVs of blasting vibration easily exceed the allowable value, thus causing damage to the structures (Singh and Roy 2010). As the distance from the explosion source increases, the PPVs rapidly decrease to a range that does not endanger the structures, and the dominant frequencies of blasting vibration tend to the natural frequency. However, when the dominant frequencies are in the natural frequency range, resonance can easily occur and threaten the stability of the structures (Heath et al. 2015). Therefore, to minimize the disturbance of blasting vibration and protect the structures, the adjustment of inherent and

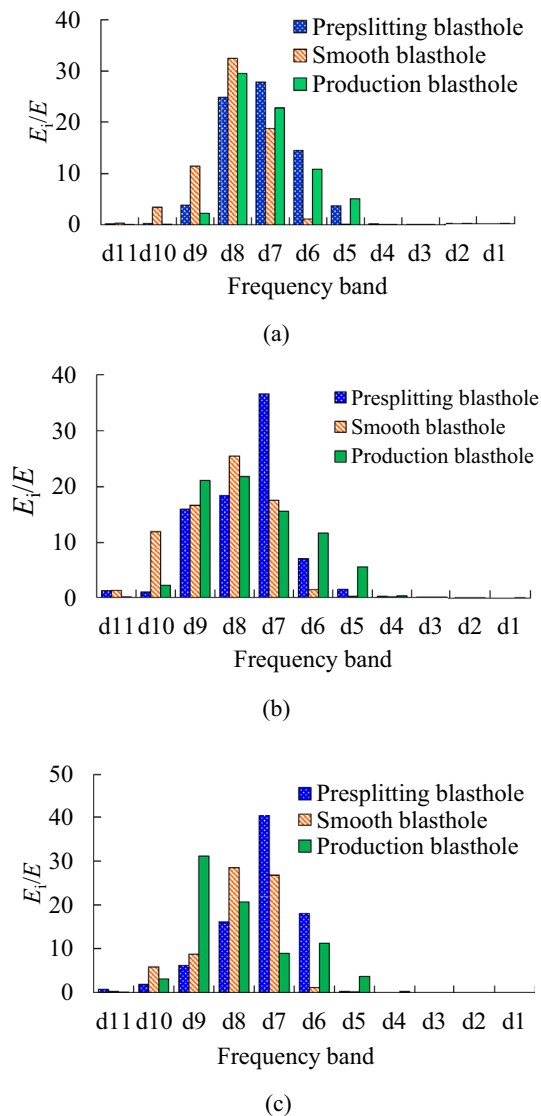


Fig. 24 Energy distribution against frequency bands at different monitoring points: **a** monitoring point #1, **b** monitoring point #2, and **c** monitoring point #3

outer blasting effects by the variations in blasting parameters can be conducted according to the distance from the explosion source. For example, when the structures are in the vicinity of the explosion sources, some optimizations, such as reducing the burden thicknesses and increasing the number of free surfaces, can be performed to enhance the outer blasting effects, so that less explosion energy is converted into vibration energy reducing the PPVs of blasting vibration. Furthermore, when the structures are in the area far from the explosion sources, it is advisable to weaken the inner blasting effects, creating a smaller plastic zone and increasing the dominant frequencies of blasting vibration, which is beneficial for protecting the structure from

the resonance. In addition, all these optimizations should be carried out in an attempt to satisfy the rock fragmentation.

6 Conclusions

Figuring out the inherent causes of vibration characteristics induced by different kinds of blastholes is significant for the safety control of blasting vibration. Taking the Baihetan dam foundation blasting excavation as a case study, the blasting parameters of various blastholes were analyzed at first stage. Then, the effects of blasting parameters on vibration responses were investigated with both theoretical analyses and numerical simulation. It was observed that since the explosives in contour blastholes are decoupled from the rock mass and laterally initiated by the detonating cord, the blasting pressure on the hole wall of contour blastholes is substantially lower, weakening the inner blasting effects in rock breakage. In addition, the presplitting blastholes are initiated in the first row to form the pre-splitting cacks. Thus, the outer blasting effects of presplitting blastholes are negligible as their burden thicknesses are larger relative to the other blastholes. The smooth blastholes are initiated after the production blastholes. Consequently, their burden thicknesses are relatively small, resulting in stronger outer blasting effects than the other two kinds of blastholes.

Horizontal smooth blasting and horizontal presplitting blasting were conducted to investigate the vibration characteristics differences in dam foundation blasting excavation. By analyzing the recorded vibration signals from the onsite experiment, it was found that the PPVs and dominant frequencies induced by presplitting blastholes were significantly higher than those induced by smooth blastholes and production blastholes due to the weaker inner and outer blasting effects of presplitting blastholes. While the PPVs and dominant frequencies induced by smooth blastholes were roughly comparable to those of production blastholes, due to the balance of their inner and outer blasting effects. The findings of the onsite experiment clearly verify the conclusions of the numerical simulation and theoretical analysis.

The differences in blasting parameters (i.e., charge structures, initiation modes, and burden thicknesses) result in variations in the proportions of the inner and outer blasting effects, which are the inherent causes for the vibration differences induced by different kinds of blastholes. In practical engineering, it is advisable to adjust the blasting parameters of various blastholes to change the proportions of the inner and outer blasting effects, thereby minimizing the blasting disturbance to the structures.

Acknowledgements This work is supported by the National Natural Science Foundation of China (52009003, 51979152), Open Foundation

of Hubei Key Laboratory of Construction and Management in Hydropower Engineering (2020KSD01), Natural Science Basic Research Program of Shaanxi (2021JQ-258), and the Fundamental Research Funds for the Central Universities, CHD (300102213702). The authors wish to express their thanks to all supporters.

Author Contributions ZH: data curation, software, and writing the original draft. GQ: conceptualization, experiment, methodology, and funding. FY: conceptualization, validation, review and editing. LW: conceptualization, methodology, and project administration. WY: methodology and supervision. YY: formal analysis and data curation. LZ: conceptualization, experiment, and validation.

Data Availability All data, models, or code that support the findings of this study are available from the corresponding author upon reasonable request.

Declarations

Conflict of interest The authors declare that they have no known competing financial or personal relationships that could have influenced the work reported in this paper.

References

- Abiodun IL, Sangki K, Olaide SH, Musa AI (2021) Blast-induced ground vibration prediction in granite quarries: an application of gene expression programming, ANFIS, and sine cosine algorithm optimized ANN. *Int J Min Sci Technol* 31(2):265–277. <https://doi.org/10.1016/j.ijmst.2021.01.007>
- Ainalis D, Kaufmann O, Tshibangu JP, Verlinden O, Kouroussis G (2016) Modelling the source of blasting for the numerical simulation of blast-induced ground vibrations: a review. *Rock Mech Rock Eng* 50(1):1–23. <https://doi.org/10.1007/s00603-016-1101-2>
- An L, Suorinen FT, Xu S, Li YH, Wang ZC (2018) A feasibility study on confinement effect on blasting performance in narrow vein mining through numerical modelling. *Int J Rock Mech Min* 112:84–94. <https://doi.org/10.1016/j.ijrmms.2018.10.010>
- Banadaki M, Mohanty B (2012) Numerical simulation of stress wave induced fractures in rock. *Int J Impact Eng* 40(1):16–25. <https://doi.org/10.1016/j.ijimpeng.2011.08.010>
- Chapman DL (1899) On the rate of explosion in gases. *Philos Mag* 47:90–104. <https://doi.org/10.1080/14786449908621243>
- Esen S, Onederra I, Bilgin HA (2003) Modelling the size of the crushed zone around a blasthole. *Int J Rock Mech Min Sci* 40(4):485–495. [https://doi.org/10.1016/S1365-1609\(03\)00018-2](https://doi.org/10.1016/S1365-1609(03)00018-2)
- Gao Q, Lu W, Leng Z, Yang Z, Zhang Y, Hu H (2019a) Effect of initiation location within blasthole on blast vibration field and its mechanism. *Shock Vib* 2019:1–18. <https://doi.org/10.1155/2019/5386014>
- Gao Q, Lu W, Yan P, Hu H, Yang Z, Chen M (2019b) Effect of initiation location on distribution and utilization of explosion energy during rock blasting. *B Eng Geol Environ* 78(5):3433–3447. <https://doi.org/10.1007/s10064-018-1296-4>
- Heath D, Gad E, Wilson L (2015) Blast vibration and environmental loads acting on residential structures: state-of-the-art review. *J Perform Constr Fac* 30(2):1–12. [https://doi.org/10.1061/\(ASCE\)CF.1943-5509.0000750](https://doi.org/10.1061/(ASCE)CF.1943-5509.0000750)
- Hu Y, Lu W, Chen M, Yan P, Yang J (2014) Comparison of blast-induced damage between presplit and smooth blasting of high rock slope. *Rock Mech Rock Eng* 47(04):1307–1320. <https://doi.org/10.1007/s00603-013-0475-7>
- Hu Y, Yang Z, Huang S, Lu W, Zhao G (2020) A new safety control method of blasting excavation in high rock slope with joints. *Rock Mech Rock Eng* 53(2):3015–3029. <https://doi.org/10.1007/s00603-020-02113-3>
- Katsabanis PD (2020) Analysis of the effects of blasting on comminution using experimental results and numerical modelling. *Rock Mech Rock Eng* 53(7):3093–3109. <https://doi.org/10.1007/s00603-020-02093-4>
- Lee EL, Hornig HC, Kury JW (1968) Adiabatic expansion of high explosive detonation products. Report UCRL-50422. <https://doi.org/10.2172/4783904>
- Lee EL, Tarver CM (1980) Phenomenological model of shock initiation in heterogeneous explosives. *Phys Fluids* 23(12):2362–2372. <https://doi.org/10.1063/1.862940>
- Leng Z, Lu W, Chen M, Fan Y, Wang G (2016) Explosion energy transmission under side initiation and its effect on rock fragmentation. *Int J Rock Mech Min* 86:245–254. <https://doi.org/10.1016/j.ijrmms.2016.04.016>
- Li M, Kemin L, Xiao S, Ding X, Sydeney C (2016) Research on effects of blast casting vibration and vibration absorption of presplitting blasting in open cast mine. *Shock Vib* 2016:1–9. <https://doi.org/10.1155/2016%2F4091732>
- Liu G, Lu W, Niu X, Wang G, Chen M, Yan P (2020) Excavation shaping and damage control technique for the breccia lava dam foundation at the Bai-He-Tan Hydropower Station: A case study. *Rock Mech Rock Eng* 53(4):1889–1907. <https://doi.org/10.1007/s00603-019-02013-1>
- Lu W, Chen M, Xiang G, Shu D, Zhou C (2012) A study of excavation sequence and contour blasting method for underground powerhouses of hydropower stations. *Tunn Undergr Space Technol* 29:31–39. <https://doi.org/10.1016/j.tust.2011.12.008>
- Lu W, Zhou J, Chen M, Yan P, Wang G (2015) Study on attenuation formula of dominant frequency of blasting vibration. *Engineering. Blasting* 21(06): 1–6. https://en.cnki.com.cn/Article_en/CJFDTOTAL-GCBP201506001.htm
- Lu W, Hu H, Yan P, Chen Y, Rong Y, Wang Z (2018) Vertical borehole shock-reflection blasting technique and its application in foundation excavation. *Chin J Mech Eng* 37(A01): 3143–3152. <https://doi.org/10.13722/j.cnki.jrme.2017.1051>
- Ma C, Wu L, Sun M (2022) Influence of free surface numbers on the energy distribution and attenuation of vibration signals of underwater drilling blasting. *Explos Shock Waves* 42(1):1–12. <https://doi.org/10.1088/1755-1315/560/1/012076>
- Riedel W, Thoma K, Hiermaier S, Schmolinske E (1999) Penetration of reinforced concrete by BETA-B-500 numerical analysis using a new macroscopic concrete model for hydrocodes. In Proceedings of 9th international symposium on interaction of the effects of munitions with structures, Strausberg, Germany, pp. 315–322
- Sanchidrián J, Segarra P, López LM (2007) Energy components in rock blasting. *Int J Rock Mech Min* 44(1):130–147. <https://doi.org/10.1016/j.ijrmms.2006.05.002>
- Sastry V, Ram Chandar K (2004) Shock tube initiation for better fragmentation: a case study. *Fragblast* 8(4):207–220. <https://doi.org/10.1080/13855140500041770>
- Shadabfar M, Gokdemir C, Zhou M, Kordestani H, Muho EV (2021) Estimation of damage induced by single-hole rock blasting: a review on analytical, numerical, and experimental solutions. *Energies* 14(1):1–24. <https://doi.org/10.3390/en14010029>
- Shi X, Chen S (2009) Explosive blasted per delay and burden effects on the time frequency characteristics of vibration induced by blast. *J China Coal Soc* 34(3): 345–349. <http://www.mtxb.com.cn/paper/4046>
- Singh S (1993) Predictions and measurement of blast vibrations. *Int J Min Reclam Env* 7(4):149–154. <https://doi.org/10.1080/09208119308964700>

- Singh PK, Roy MP (2010) Damage to surface structure due to blast vibration. *Int J Rock Mech Min* 47:949–961. <https://doi.org/10.1016/j.ijrmms.2010.06.010>
- Singh PK, Roy MP, Paswan RK (2014) Controlled blasting for long term stability of pit-walls. *Int J Rock Mech Min* 70:388–399. <https://doi.org/10.1016/j.ijrmms.2014.05.006>
- Sun P, Lu WB, Zhou J, Huang X, Chen M, Li Q (2021) Comparison of dominant frequency attenuation of blasting vibration for different charge structures. *J Rock Mech Geotech Eng* 14(2):448–459. <https://doi.org/10.1016/j.jrmge.2021.07.002>
- Torano J, Rodriguez R, Diego I, Rivas JM, Casal MD (2006) FEM models including randomness and its application to the blasting vibrations prediction. *Comput Geotech* 33(1):15–28. <https://doi.org/10.1016/j.compgeo.2006.01.003>
- Wang G, Zhang S (2014) Damage prediction of concrete gravity dams subjected to underwater explosion shock loading. *Eng Fail Anal* 39:72–91. <https://doi.org/10.1016/j.engfailanal.2014.01.018>
- Xie L, Lu W, Zhang Q, Jiang Q, Chen M, Zhao J (2017) Analysis of damage mechanisms and optimization of cut blasting design under high in-situ stresses. *Tunn Undergr Space Technol* 66:19–33. <https://doi.org/10.1016/j.tust.2017.03.009>
- Yang J, Lu W, Jiang Q, Yao C, Zhou C (2016) Frequency comparison of blast-induced vibration per delay for the full-face millisecond delay blasting in underground opening excavation. *Tunn Undergr Space Technol* 51:189–201. <https://doi.org/10.1016/j.tust.2015.10.036>
- Yang L, Yang A, Chen S, Fang S, Xie H (2021) Model experimental study on the effects of in situ stresses on pre-splitting blasting damage and strain development. *Int J Rock Mech Min* 138(4):1–9. <https://doi.org/10.1016/j.ijrmms.2020.104587>
- Yang F, Li H, Liu Y, Zhou F, Xia X, Hao Y (2012) Comparative study on vibration characteristics of rock mass induced by bench blasting and pre-splitting blasting. *J China Coal Socy* 37(8): 1285–1291. <https://doi.org/10.13225/j.cnki.jccs.2012.08.003>
- Yilmaz O, Unlu T (2013) Three dimensional numerical rock damage analysis under blasting load. *Tunn Undergr Space Technol* 38:266–278. <https://doi.org/10.1016/j.tust.2013.07.007>
- Zeng Y, Li H, Xiang X, Liu B, Zuo H, Jiang J (2018) Blast-induced rock damage control in Fangchenggang Nuclear Power Station, China. *JRMGE* 10(05):914–923. <https://doi.org/10.1016/j.jrmge.2018.04.010>
- Zhang Y, Lu W, Chen M (2013) Dam foundation excavation techniques in China: a review. *JRMGE* 5(6):460–467. <https://doi.org/10.1016/j.jrmge.2013.08.002>
- Zhong G, Fang Y, Xu G (2008) Study on blasting vibration effect assessment of structure based on wavelet transform. *J Vibrat Shock* (08): 121–124. https://en.cnki.com.cn/Article_en/CJFDTOTAL-ZDCJ200808033.htm
- Zhou Z, Chen R, Cai X, Jia J, Wang W (2019) Comparison of presplit and smooth blasting methods for excavation of rock wells. *Shock Vib*. <https://doi.org/10.1155/2019/3743028>

Publisher's Note Springer Nature remains neutral with regard to jurisdictional claims in published maps and institutional affiliations.

Springer Nature or its licensor (e.g. a society or other partner) holds exclusive rights to this article under a publishing agreement with the author(s) or other rightsholder(s); author self-archiving of the accepted manuscript version of this article is solely governed by the terms of such publishing agreement and applicable law.